Chapter

Effect of Laminar Flow on the Corrosion Activity of AA6061-T6 in Seawater

Gloria Acosta, Lucien Veleva, Luis Chávez and Juan L. López

Abstract

The electrochemical behaviour and surface changes on AA6061-T6 alloy exposed to Caribbean seawater from the Cozumel Channel for 30 days under laminar flow (0.1 ms^{-1}) were studied, these contrasting then with stationary conditions. Open circuit potential monitoring and electrochemical current fluctuations, considered as electrochemical noise (EN), were employed as two nondestructive methods. The calculated corrosion current, based on Rn, was one order higher in laminar flow. The fluctuations of current were transformed in the frequency domain. Their power spectral density (PSD) plots were obtained in order to gain information concerning the dynamic of the spontaneous release of energy during the corrosion process. The value of the exponent β in PSD graphs suggested that the localised corrosion on AA6061-T6 surface occurs as a persistent stationary process, which dynamic is controlled by oxygen diffusion. The changes in the morphology and elemental composition of the formed layers revealed that the localised attacks occurred in the vicinity of intermetallic particles rich in Fe and Cu, which act as cathodes.

Keywords: aluminium alloy 6061-T6, seawater, laminar flow, intermetallic particles, electrochemical current noise

1. Introduction

Aluminium alloy (AA) 6061-T6 is popular as a nonferrous material for structures in seawater [1] and is characterised by various properties, such as strength-to-weight ratio, extrudability—particularly for the manufacture of profiles with complex geometry, low thermal expansion coefficient, good wear resistance and corrosion resistance [2]. The alloy presents good corrosion resistance in many environments having neutral pH, because of the formation of protective amorphous aluminium oxide film on its surface of approximately 2–3 nm thickness and is insoluble in water [3, 4]. The addition of alloying elements to aluminium increases its mechanical properties [5]; however, the precipitated intermetallic particles (IMPs) have a harmful effect on the corrosion resistance of the Al alloys [4, 6–10]. IMPs present electrochemical behaviour different from the alloy matrix, and they may be classified in two types: cathodic and anodic [7, 9–12]. The electrochemically active anodic particles are rich in Mg, Si and Al, with Mg preferential dissolution, leaving a cavity in the oxide layer, while the cathodic particles are rich in Fe, Si and Cr, acting as preferential sites for oxygen reduction.

The localised corrosion becomes greater in the presence of aggressive ions, such as chlorides [4, 13–15], and corrosion pits initiate in oxide film sites, weakened by chloride attack. Moreover, the heterogeneity of the surface could result in favourable nucleation sites.

Seawater is a complex electrolyte of different ions, with a high salinity (3.5%, density 1.023 g/cm^3 at 25°C), which causes damage to metals in a short time [16, 17]. The principal parameters that affect the corrosion behaviour of metals immersed in this electrolyte are oxygen content, dissolved mineral salts, pH, temperature, specific contaminants and flow velocity [16, 18].

The characterisation of the corrosion process requires electrochemical nondestructive techniques, and the preferred methods are those that do not apply external polarisation. The monitoring of the open circuit potential (φ_{corr}, free corrosion potential) or corrosion current is one of these and is easy to handle. Fluctuations may be interpreted as electrochemical noise (EN), which is useful for the purposes of corrosion mechanism characterisation. Electrochemical noise is presented by random fluctuations of corrosion potential or current, typically with frequencies below 10 Hz and low amplitude [19]. This technique can provide information concerning the nature of the corrosion process and the rate thereof. The main sources of EN observed in corrosion systems are attributed to microscopic and macroscopic events [19–21]. EN measurements can be performed under corrosion potential or any constant potential/current, depending on the research objective, to analyse the corrosion mechanism and obtain the corrosion rate [20].

EN measurements can be analysed transforming the data in the frequency domain by fast Fourier transform (FFT) to obtain power spectral density (PSD) [22, 23]. PSD plots display a slope, β exponent, which enables the differentiation between series with fractional Gaussian noise (*fGn*, β from −1 to 1) and fractional Brownian motion (fBm, β from 1 to 3). The *fGn* is a stationary process, and the fBm is nonstationary [24, 25]. The β exponent is a parameter correlated with the strength of persistence in a process [26]. In our previous studies, EN technique was carried out to characterise the first stages of corrosion in stationary seawater of copper [27], aluminium [28] and aluminium alloys [29], as well as the initial stages of AZ31B Mg alloy in simulated body fluid [30].

The object of this study is to investigate the electrochemical behaviour and surface changes on AA6061-T6 alloy, exposed to Caribbean seawater (Cozumel Channel) under laminar flow, contrasting these with stationary flow. Two nondestructive electrochemical methods were used to test the corrosion resistance of the alloy. The corrosion current and φ_{corr} were considered as EN and transformed in the frequency domain, in order to gain information on the dynamics of the spontaneous release of energy during the corrosion process. X-ray photoelectron spectroscopy (XPS) measurement was employed to analyse the composition of the formed corrosion layers, as well as SEM-EDS surface analysis. To the best of own knowledge, there is still no study on the initial stages of localised corrosion of AA6061-T6 alloy in laminar flow conditions.

2. Experimental

2.1 Materials

The nominal composition of AA6061-T6 (Metal Plastic Mexicali) was (wt%) 1.10% Mg, 0.5% Fe, 0.4% Si, 0.31% Cu, 0.19% Cr, 0.07% Zn and 0.05% Ti and the remainder Al. The seawater was extracted from the Caribbean Cozumel Channel, at 10 km offshore, to minimise the effect of human pollution, and a depth of 10 m. The

seawater composition and physicochemical properties were as follows: salinity 36.4 g L^{-1}, chlorides 20.12 g L^{-1}, sulphates 2.82 g L^{-1}, nitrates 0.48 μmol/L, nitrites 0.18 μmol/L, ammonia 0.99 μmol/L, pH 7.3, dissolved oxygen 5.8 mg L^{-1} and conductivity 51.6 mS.

Samples of 1 cm^2 were embedded in Epofix resin as working electrodes for electrochemical tests. In addition, samples of 1 cm^2 were cleaned with ethanol and immersed in 100 mL of seawater (triplicated) under flow conditions, for 0, 5, 15 and 30 days, respectively. Before exposure, the specimens were ground with silicon carbide paper to 4000 grit, using distilled water as lubricant. They were washed with distillated water and dried in air.

2.2 Laminar flow of seawater

The speed range found in the Cozumel Channel indicates that the ocean current speed oscillates between 0.1 and 1 m s^{-1}. The tubing employed to connect the peristaltic pump (LAMBDA Laboratory Instrument) with the electrochemical cell has a diameter of 6 mm, and using the lower limit of the flow speed (0.1 m s^{-1}), the calculated Reynolds number was 622.97, which corresponds to laminar hydrodynamic flow [31]. The dimensionless N_{Re} characterises the diffusion-dependent system and is governed by the ratio of the inertial forces acting on the fluid to the viscous forces:

$$N_{Re} = \frac{\rho \overline{u} d}{\mu} \tag{1}$$

where ρ is the fluid density (seawater, 997.8 kg m^{-3}), $\overline{u}$ is the flow speed (0.1 m s^{-1}), d is the tubing diameter (6 mm) and μ is the seawater viscosity (0.961×10^{-3} N s m^{-2}). All experiments were carried out at 21°C.

2.3 Surface analysis

AA6061-T6 samples were characterised before and after exposure in seawater by SEM-EDS (Philips-XL and ESEM-JEOL JSM-7600F), in order to observe the microstructure and elemental changes on their surface. Corrosion products formed on AA6061-T6 sample surfaces were identified through X-ray photoelectron spectroscopy (XPS, K-alpha, Thermo Scientific, Waltham, MA, USA). In addition, corrosion products were removed in accordance with ASTM G1-90 standard [32], and the alloy surfaces were reexamined.

2.4 Electrochemical tests

A multiport electrochemical cell kit (Gamry Instruments, 1 L total volume) and a Gamry PCI4G750-52103 potentiostat were used for all electrochemical measurements. The experimental setup employed was according to ASTM G199-09 standard [33]: two identical AA6061-T6 working electrodes (WEs) connected to a zero resistance ammeter (ZRA) and a saturated calomel electrode (SCE, Hg^{2+}/Hg_2Cl_2 = 0.244 V) as reference electrode. The electrodes were immersed in an electrochemical cell with seawater, employed as test electrolyte. All tests were carried out in laminar and stationary flow conditions up to 30 days. EN data were collected at different times during 3 h, initial, 1, 5, 15 and 30 days in OCP, with a sampling frequency of 10 Hz. The obtained data of current and potential fluctuations were plotted vs. time. The current fluctuations were considered as EN and processed in the frequency domain by fast FFT to graph PSD. The PSD as a function of low

frequencies was analysed on bi-logarithmic scale (10^{-3} –1 Hz) of power per unit frequency (A^2/Hz) vs. frequency (Hz). These procedures allowed the fitting of a straight line and obtention of the β slope. The β value characterises the corrosion mechanism on AA6061-T6 surface. The processing of data was realised with Electrochemical Signal Analyser V.7.0.1 software (Gamry Instruments, Philadelphia, PA, USA). All measurements were checked in triplicate.

2.4.1 Energy spectral density

The energy spectral density expresses how the energy of a time series is dispersed with a frequency; it can reflect the change in system dynamic. For a signal X(t) the energy EE is [34]

$$E = \int_{-\infty}^{\infty} |x(t)|^2 dt \tag{2}$$

For signals with a finite total energy, an equivalent expression for the energy is expressed as

$$E = \int_{-\infty}^{\infty} |x(t)|^2 dt = \int_{-\infty}^{\infty} |\hat{x}(f)|^2 df \tag{3}$$

And using the Fourier transform of the signal:

$$\hat{x}(f) = \int_{-\infty}^{\infty} e^{-2\pi i f t} x(t) df \tag{4}$$

where f is the frequency in Hz.

The integral on the right-hand side of Eq. (3) is the energy of the signal, and the integrand $|\hat{x}(f)|^2$ describes the energy per unit frequency contained in the signal (ESD).

3. Results and discussion

3.1 Surface analysis

Figure 1 shows SEM images of the as-received specimen of 6061-T6 aluminium alloy surface. Small precipitates (labelled as A, B, C) may be seen (**Figure 1b**). In accordance with EDS, presented in **Table 1**, these precipitates correspond to particles rich in Fe and could be considered as elements of the following phases: Al_3Fe, Al–Si–Mn–Fe and α-Al(Fe, Mn, Cu) [9, 10, 35]. The elemental composition of the surface layer is indicated by zone D.

Figure 2a presents the SEM image of the film formed on the surface of the sample after 5 days of immersion in seawater from the Cozumel Channel under laminar flow. It can be clearly seen that the passive layer begins to break down around the alloying elements (**Figure 2b**). Probably, this layer is less protective in the vicinity of the intermetallic particles, causing the formation of local electrochemical cells with the Al matrix. EDS analysis, **Table 2**, confirmed the presence of particles mentioned above. According to EDS (**Table 2**), zone A is characterised by its higher content of Al, O and Cl, which could relate to corrosion products. According to previous studies, at pH > 8.5, $Al(H_2O)_6^{3+}$ cations appear, while in the range of pH 4.5–8.5, $Al(OH)_3$ predominates [36, 37]. In chloride solutions,

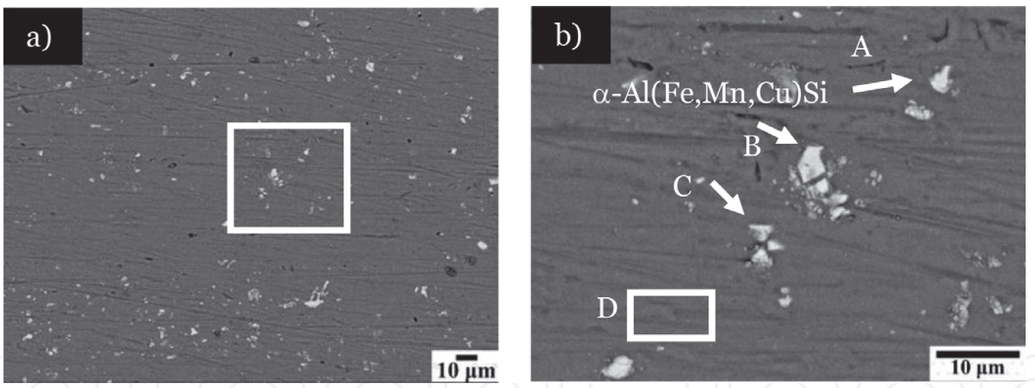

Figure 1.
(a) SEM images (×500) of AA6061-T6 surface before immersion in Caribbean seawater and (b) zoom zone (×2000).

Element	C	O	Mg	Al	Si	Cr	Mn	Fe	Cu
A	2.4	3.3	—	60.3	6.5	1.3	1.6	23.7	0.9
B	2.3	2.7	—	59.3	7.4	1.3	1.5	24.2	1.3
C	2.2	4.5	—	71.7	4.8	0.6	0.9	14.6	0.7
D	2.0	2.1	1.7	93.7	0.5	—	—	—	—

Table 1.
EDS analysis (wt%) of reference aluminium alloy 6061-T6 surface.

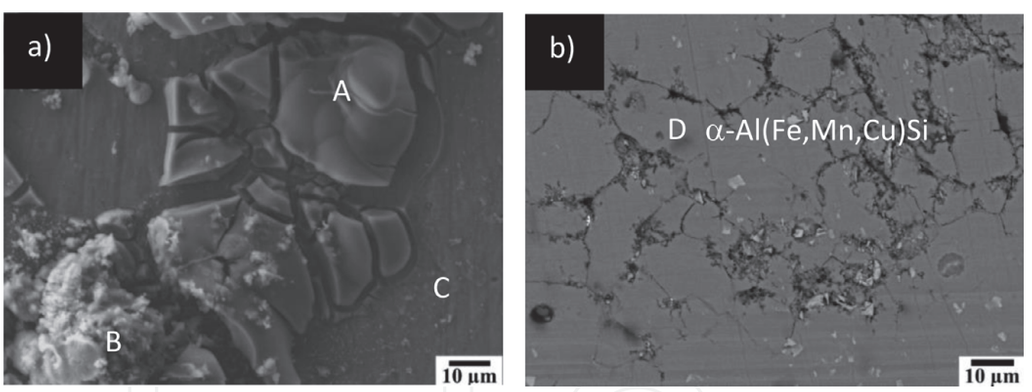

Figure 2.
SEM images of AA6061-T6 surface after exposure in Caribbean seawater under laminar flow for 5 days (a) and (b) after removal of corrosion layer.

(a)										
Element	**C**	**O**	**Na**	**Mg**	**Al**	**Si**	**S**	**Cl**	**K**	**Ca**
A	—	47.4	0.7	1.2	25.1	—	1.8	23.3	—	0.5
B	6.4	56.6	1.9	1.0	29.2	—	0.4	0.5	0.5	3.5
C	4.4	11.5	—	0.8	81.2	0.4	0.4	0.3	0.8	0.2
(b)										
Element	**C**	**O**	**Mg**	**Al**	**Si**	**Cr**	**Mn**	**Fe**	**Cu**	
D	10.9	4.7	0.4	58.0	5.8	0.6	1.2	17.6	0.8	

Table 2.
(a) EDS analysis (wt.%) of aluminium alloy 6061-T6 surface after 5 days of exposure in Caribbean seawater under laminar flow at 21°C and (b) after removal of corrosion products.

aluminium metal ionises rapidly to the Al^{3+} ion, which also hydrolyses very rapidly (owing to the negative potential value) [38]. Both of these Al cations can react with chloride ions and form $AlCl_3$ soluble in water (31.77 wt%) [39]; this is converted later to a relatively stable species of basic aluminium chloride ($AlCl_3 \bullet H_2O$), transformed slowly to $Al(OH)_3$ and finally to $Al_2O_3 \bullet H_2O$, an important corrosion product for the repassivation process of the aluminium surface [38].

Based on EDS analysis, in zone B in addition to oxygen and aluminium, elements of calcium and carbon were present, both possibly as a part of a $CaCO_3$ precipitate, originating from seawater. Meanwhile, the layer in zone C maintained a composition similar to that of the alloy, which indicates that the corrosion process was still beginning on the surfaces of similar areas.

After removal of the layer of corrosion products (**Figure 2b**), area damaged by pitting and cracking was observed on the alloy surface. However, some precipitates remained on the surface of AA6061-T6, which according to EDS (**Table 2**) correspond to cathodic particles rich in Fe, α-Al(Fe,Mn,Cu)Si, which promoted the preferential dissolution of the aluminium matrix (local alkalisation) [10].

Figure 3 compares SEM images of the aluminium alloy 6061-T6 after exposure at 30 days in laminar flow (**Figure 3a** and **c**) and stationary flow (**Figure 3b** and **d**). In these micrographs, the products formed on the surfaces of the alloy (**Figure 3a** and **b**) can be seen and compared, whose EDS analysis is summarised in **Table 3**. In laminar flow (**Figure 3a**), the segregation of particles rich in Cu (particles A) with the presence of O and Al could be considered as the phases of Al_2Cu, AlMgSiCu (Q-phase) and Al_7Cu_2Fe; both relatively resistant to corrosion, because they are nobler than the aluminium matrix [4, 12]. Q-phase acts as a cathode and does not contribute to intergranular corrosion when it is not connected to any other Cu particle. Otherwise, the Q-phase as cathode promotes the development of intergranular corrosion, initiated in the presence of chloride ions (NaCl). In the corrosion layer, particles without Cu appeared (particles B), rich in Fe, Al and Mg,

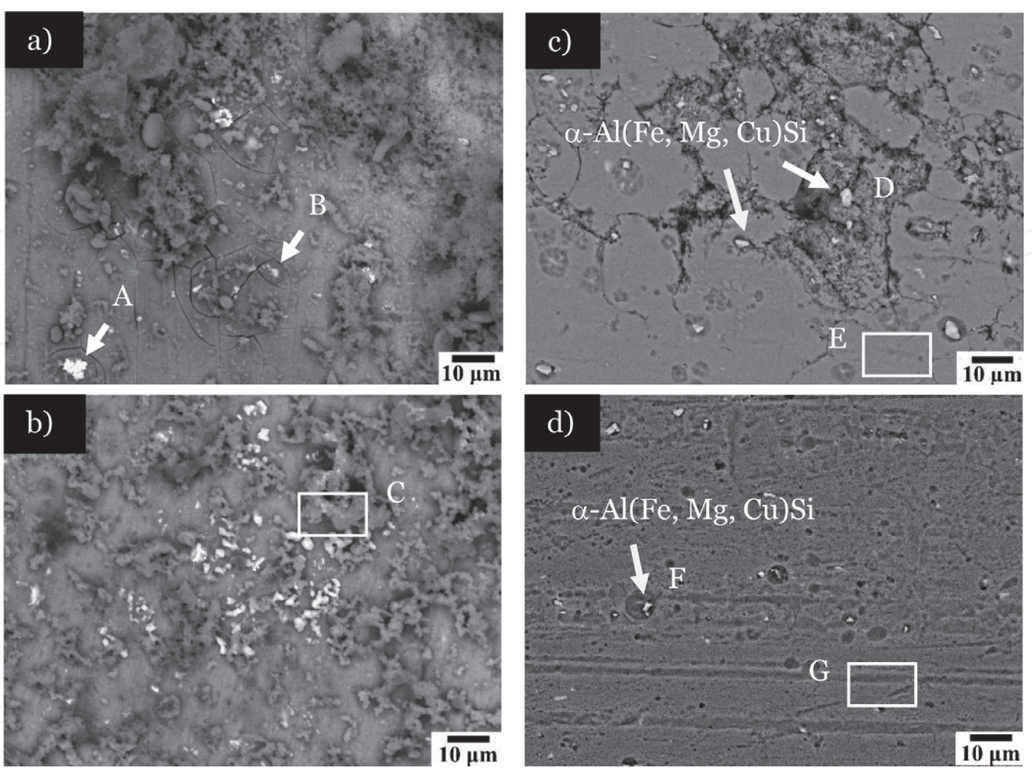

Figure 3.
SEM images of AA6061-T6 surface after 30 days of exposure in Caribbean seawater, (a) laminar and (b) stationary flow conditions; after removal of corrosion products, (c) laminar and (d) stationary flow conditions.

					(a)							
Element	**C**	**O**	**Na**	**Mg**	**Al**	**Si**	**Cr**	**Mn**	**Cl**	**Ca**	**Fe**	**Cu**
A	3.3	22.3	2.2	3.3	10.2	0.7	—	—	1.0	0.3	1.0	55.7
B	4.2	31.3	1.7	1.8	39.6	3.9	0.5	0.8	0.8	0.5	14.2	0.7
C	12.7	44.9	0.5	3.0	37.8	0.1	—	—	0.5	0.5	—	—
					(b)							
D	4.1	—	—	—	63.3	6.0	1.0	1.2	1.5	—	21.8	1.1
E	5.7	4.4	—	0.5	84.6	3.2	0.7	0.9	—	—	—	—
F	5.7	1.5	—	—	69.6	5.1	1.3	1.0	—	—	15.0	0.8
G	5.8	4.6	—	0.7	88.2	0.4	0.2	—	—	—	—	—

Table 3.
EDS analysis (wt%) of aluminium alloy 6061-T6 surfaces: (a) after 30 days of exposure in seawater under laminar flow and (b) after removal the layer of corrosion products.

which could be attributed to the following phases, Al–Si–Mn–Fe and Al–Mg–Si, reported for aluminium alloy series 6xxx [35]. Zone C of the layer formed under stationary flow (**Figure 3b**) presented a similar composition of the alloy (**Table 3**), however, with the oxide layer of $Al_2O_3 \cdot H_2O$ on the alloy surface 6061-T6, as a transformation product of basic aluminium ($AlCl_3 \cdot H_2O$) in the presence of NaCl [38]. This layer is part of the entire surface (**Figure 3a**), since the three zones (A, B and C) have a high oxygen content (**Table 3**) [4].

Figure 3c corresponds to the SEM image of the aluminium alloy 6061-T6 exposed in seawater at 30 days with flow, after removal of the layer of corrosion products. An area on the surface damaged by cracking and fissures can be observed, while the surface exposed to seawater without flow (**Figure 3d**) shows less damage, with pitting holes of several diameters. In contrast, on the surface exposed to laminar flow for this same time period, the pits are not clearly observable, but localised corrosion damage appeared in the form of cracks and fissures. This effect is due to the seawater flow, which accelerates the corrosion process, causing detachment of the destroyed passive layer and the appearance of new "fresh" areas, where the oxygen diffuses and is the oxidising agent in the cathodic corrosion reaction. It is also observed that on both surfaces (**Figure 3c** and **d**), some particles remained (named as D and F), and according to EDS (**Table 3**), they correspond to cathodic rich in Fe [7], reported in the reference sample as α-Al(Fe,Mn,Cu)Si [35]; these intermetallic particles promoted the preferential dissolution of the aluminium matrix [40, 41].

3.2 OCP (free corrosion potential, φ_{corr}) measurements

Figure 4 compares the φ_{corr} fluctuations of AA6061-T6 specimens exposed for different periods of times (0, 5 and 30 days) under laminar flow conditions (**Figure 4a**) and without flow (**Figure 4b**). The average values are summarised in **Table 4**. The trends in the changes, towards more or less negative values, are a response to the transformations that have occurred on the surface of the aluminium alloy with the advance of the corrosion process. These are in the morphology, elemental composition of the layers formed, as well as the type of localised corrosion attack discussed previously. It can be seen (**Table 4**) that the initial values of φ_{corr} are relatively similar, being 30 mV nobler in respect of the exposed surface in laminar flow. At 5 days, which implies the initial destruction of the passive layer (**Figure 2a**), the φ_{corr} is 100 mV more negative with laminar flow than under

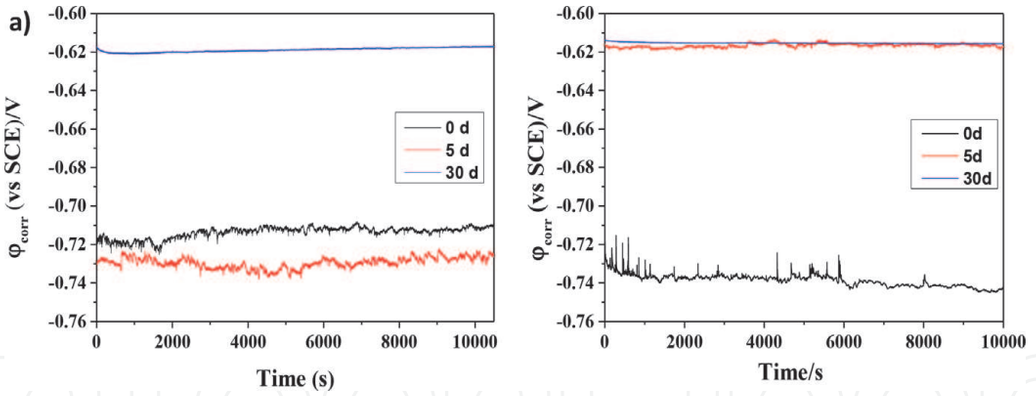

Figure 4.
Free corrosion potential (φ_{corr}) values of AA6061-T6 samples in Caribbean seawater during 30 days: (a) with laminar and (b) stationary flows.

Exposure time/days	φ_{corr} vs. SCE/mV (laminar flow)	φ_{corr} vs. SCE/mV (stationary flow)
0	−713 ± 2.80	−741 ± 16.40
5	−729 ± 2.70	−619 ± 0.95
30	−618 ± 1.00	−614 ± 0.28

Table 4.
Average of free corrosion potential (φ_{corr}) values for AA6061-T6 in Caribbean seawater under laminar and stationary flows at different times.

stationary flow. At 30 days, the φ_{corr} values in both seawater conditions (with and without laminar flow) are very similar (**Table 4**). However, when the product layer was removed (**Figure 3c** and **d**), the SEM images revealed a greater localised attack on the aluminium surface under laminar flow (**Figure 3c**), while in the absence of flow, this attack has been less aggressive, presenting shallow pits. Free corrosion potential (φ_{corr}) tendency towards more or less negative values indicates periods of corrosion activation or repassivation of the surface, both facts related to the characteristics of the layers formed [4, 42].

3.3 Surface characterisation by XPS

In order to identify the composition of the corrosion product layer created on the alloy surface after 30 days of exposure in laminar flow, XPS analysis was carried out on the specimen immersed, taking into account that aluminium corrosion products were not provided by XRD analysis as crystalline phases and are possibly amorphous.

Figure 5 shows the full XPS spectrum of the corrosion products formed on the aluminium alloy surface of 6061-T6. The XPS spectrum revealed signals of Mg, Na, O, Cl, C, Si and Al, which accord with EDS analysis. The high-resolution peak for Al2p, situated at 74.38 eV, has been associated with the presence of aluminium hydroxide [$Al(OH)_3$] [43], possibly derived from the transformation of basic aluminium chloride ($AlCl_3 \cdot H_2O$) [38]. On the other hand, the signal of O1s centred in 531.88 eV could be attributed to aluminium oxide (Al_2O_3), an important product of the repassivation process of the aluminium surface.

3.4 Electrochemical noise measurement

Figure 6 shows the current oscillations, and it can be seen that at the beginning of the experiment (0 days), the current density of AA6061-T6 surface immersed in

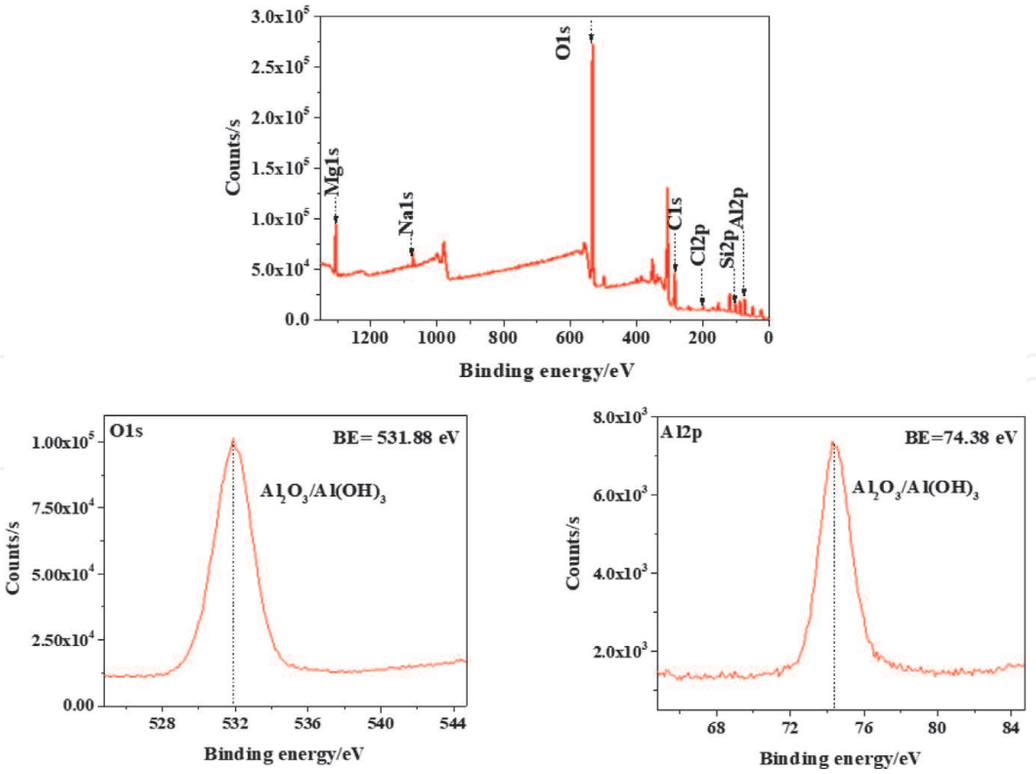

Figure 5.
Overview XPS spectra acquired from AA6061-T6 after 30 days of immersion in Caribbean seawater with laminar flow.

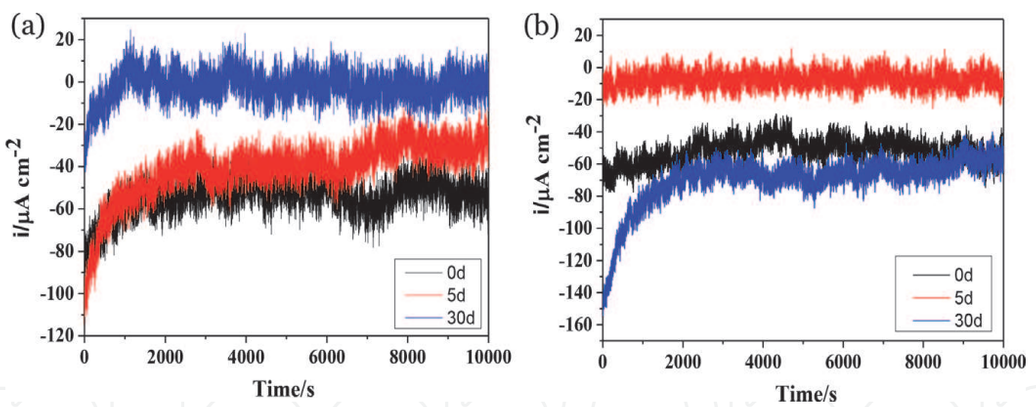

Figure 6.
Current density fluctuation for AA6061-T3 immersed in Caribbean seawater up to 30 days under (a) laminar and (b) stationary flows.

laminar flow of seawater is higher in ≈50 μA cm^{-2} than that current in stationary flow. This suggested that the corrosion of the aluminium alloy 6061-T6 surface in laminar flow initiates faster, when the oxide layer on the alloy begins to break down. However, at the end of the experiment (30 days), the current value diminished suddenly, compared with the initial values. However, in stationary flow the current shifted to one order higher values than those in laminar flow, suggesting an acceleration of the corrosion process at that period of time [44]. Conversely, the current oscillations in stationary conditions (**Figure 6b**) presented slow variations, while for flow conditions (**Figure 6a**), intense current fluctuations were acquired with greater amplitude, which suggest greater corrosion [45]. The observed current oscillations registered in (μA cm^{-2}) (**Figure 6**) correspond to the variation of the free corrosion potential (φ_{corr}) values in several mV (**Figure 4**).

The corrosion current density was calculated from the value of polarisation resistance R_p (on the assumption that R_p is equivalent to polarisation resistance

	R_p/kΩ cm^2		i_{corr} /μA cm^{-2}	
Time/d	**Laminar flow**	**Stationary flow**	**Laminar flow**	**Stationary flow**
0	3.65	23.46	7.12	1.11
5	2.24	17.5	11.60	1.49
30	1.44	19.3	18.08	1.35

Table 5.
Polarisation resistance (R_p) and corrosion current density values for AA6061-T6 immersed up to 30 days in Caribbean seawater with laminar and stationary flows.

	CR/mm year^{-1}	
Time/d	**Laminar flow**	**Stationary flow**
0	0.08	0.012
5	0.13	0.016
30	0.20	0.014

Table 6.
Corrosion rate of AA6061-T6 in Caribbean seawater from the Cozumel Channel under laminar and stationary flows.

noise R_n) obtained by ECN tests, according to the Stern-Geary equation (Eq. (5)). R_n is calculated by dividing the standard deviation of potential by standard deviation of current (the potential noise can be modelled as the action of the current noise on the metal-solution impedance):

$$i_{corr} = \frac{B}{R_p} = \frac{1}{R_p} x \frac{b_a b_c}{2.303\,(b_a + b_c)} \tag{5}$$

where R_p is the polarisation resistance and b_a and b_c are the Tafel coefficients. In this research, the B value employed was 0.26 V, taking common values for b_a and b_c of aluminium alloys [46, 47]. The calculated values (**Table 5**) show that the corrosion current of AA6061-T6 increases with the time of exposure, being more than one order higher when the alloy is exposed under laminar flow of seawater, while in stationary conditions, it maintains almost similar values up to 30 days.

Subsequently, Faraday's law was applied to calculate the corrosion rate (CR, **Table 6**) in the following form:

$$CR = \frac{i_{corr} K E_w}{\rho A} \tag{6}$$

where E_w stands for the equivalent mass of AA6061-T6, I_{corr} is the corrosion density (A cm^{-2}), ρ is the metal density, K is a constant (3272 mm/A cm year) and A is the exposed specimen area (1 cm^2) [48].

The corrosion rate values presented in **Table 6** indicate that under laminar flow, the values varied 0.08 and 0.20 mm per year, while in stationary conditions, they were between 0.012 and 0.162 mm per year.

With the statistical data obtained from the corrosion current, the pitting index (PI) [19] was calculated in order to reveal AA606-T6 susceptibility to localised corrosion for the laminar and stationary:

$$PI = \sigma_i (i_{rms})^{-1} = (639.17\,nA)(666.42\,nA)^{-1} = 0.96 \tag{7}$$

where σ_i is the standard deviation and i_{rms} the main square root of current noise.

Values of PI above 0.1 may indicate localised corrosion [20, 49]. The pitting indexes are shown in **Table 7**. Thus, the calculated PI value suggests that at the end of the experiment (30 days), for both flow cases, AA606-T6 showed pitting corrosion, approximately four times higher in flow conditions, reaching PI = 0.96. These facts agree with the SEM images (**Figure 3**) comparing the corrosion attacks on AA6061-T6 exposed to both flow conditions.

The current fluctuations, considered as EN, were transformed into the frequency domain to estimate PSD slopes (β exponent). **Figure 7** compares the PSD plots in bi-logarithmic scale, corresponding to AA6061-T6 surfaces after 30 days of exposure in seawater under laminar and stationary flows. In each case, the β exponent decreases as the frequency increases, and this fact could be associated with the advance of the localised corrosion attacks on the alloy surface [34]. At 30 days, β values are similar in laminar and stationary flows (1.0 and 0.94, respectively) and may be attributed to the fractional Gaussian noise (*fGn*), associated with a persistent process [26]. This type of noise (*fGn*) is considered also as a stationary process [24].

Figure 8 shows the spontaneous energy E during the corrosion process. At the beginning, after 5 days the energy was of an order of magnitude higher in laminar flow (1.1×10^{-4}). This fact is consistent with the SEM image presented in **Figure 2**, which showed the accelerated corrosion process causing severe damage to the alloy surface exposed to laminar flow.

However, at the end of the experiment (30 days), the energy diminished in magnitude, being very similar in the order of 10^{-7}, for both flows, probably on account of the formation of layers of corrosion products with different characteristics that act as a physical barrier on the alloy surfaces, slowing down the corrosion attack.

	σ_i/nA		i_{rms}/nA		Pitting index	
Time/days	**Laminar**	**Stationary**	**Laminar**	**Stationary**	**Laminar**	**Stationary**
0	772	639	5462	5255	0.14	0.12
5	1279	1146	4252	2866	0.30	0.40
30	639	1471	666	6733	0.96	0.22

Table 7.
Pitting index of AA6061-T6 immersed for 30 days in Caribbean seawater (Cozumel Channel) under laminar and stationary flows.

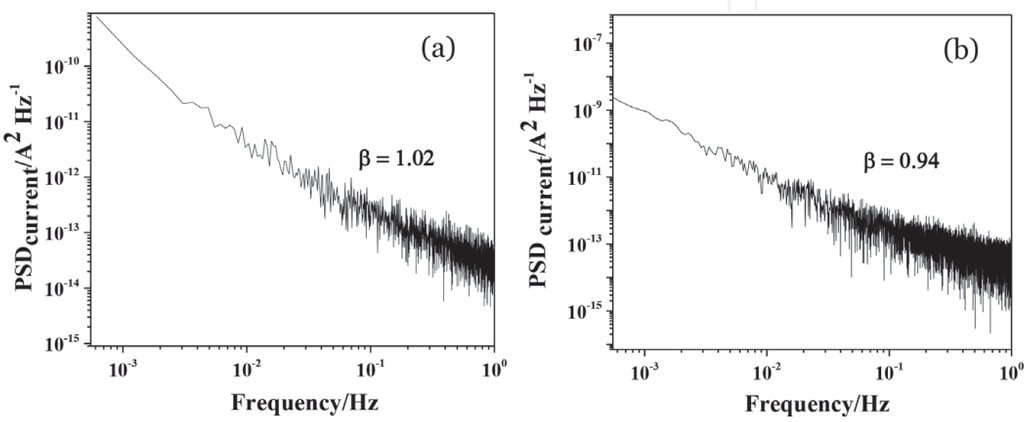

Figure 7.
Released energy (E) from AA6061-T6 surface after immersion in seawater under laminar flow, (a) at 5 days and (b) after 30 days of exposure; stationary flow, (c) at 5 days and (d) after 30 days of exposure.

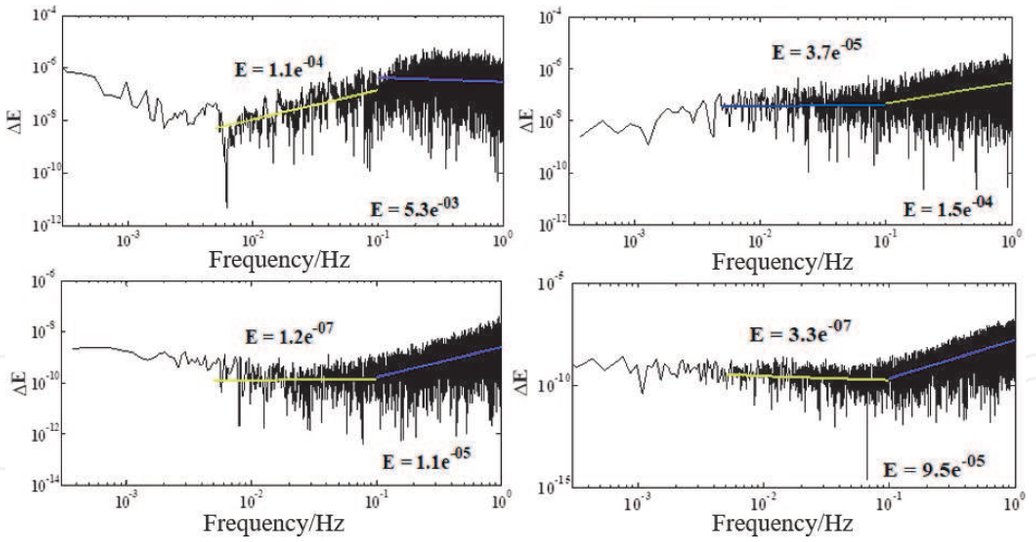

Figure 8.
Energy (E) from AA6061-T6 surface after immersion in seawater under laminar flow, (a) at 5 days and (b) after 30 days of exposure; stationary flow, (c) at 5 days and (d) after 30 days of exposure.

4. Conclusions

1. The initial electrochemical activity of 6061-T6 aluminium alloy surface, immersed in Caribbean seawater, was studied for 30 days under laminar flow (0.1 m s^{-1}, 21°C). The changes in the morphology and elemental composition of the formed layers have revealed localised corrosion (fissures and deep cracks) in the vicinity of intermetallic particles rich in Fe and Cu, which act as cathodes. The attack was less aggressive in stationary seawater, with shallow pits occurring on the surface at 30 days of exposure.

2. The calculated values showed that the corrosion current (icorr) of AA6061-T6 increases with the time of exposure more than one order higher when the alloy is exposed under laminar flow of seawater (7.12–18.08 μA cm^{-2}), while in stationary conditions, it maintains almost similar values (17.51–19.32 μA cm^{-2}). With the statistical data obtained from the corrosion current, the calculated pitting index (PI) revealed that AA606-T6 is four times more susceptible to localised corrosion in seawater under laminar flow (PI = 0.96), compared to that in stationary conditions (PI = 0.22). The estimated PSD slopes (β exponent) of the current fluctuations transformed into the frequency domain revealed that in laminar and stationary flows (β = 1.0 and 0.94, respectively), the electrochemical corrosion may be attributed to the fractional Gaussian noise (fGn), associated with a persistent stationary process.

3. The spontaneous energy release in the initial stages is one order higher in laminar flow ($\Delta E = 1.1 \times 10^{-4}$). However, at the end of the experiment (30 days), the energy diminished in magnitude, being very similar in an order of 10^{-7}, for both flows, probably on account of the formation of layers of corrosion products with different characteristic, which act as a physical barrier on the alloy surfaces, slowing down the corrosion attack.

4. The observed effect of the laminar seawater flow on the AA6061-T6 corrosion process should be considered as a consequence of the facilitated diffusion of the oxygen at the metal-seawater interface, resulting in specific transformation

in the composition of the formed corrosion layers. The presented surface SEM-EDS and XPS analysis agree positively with the results obtained with both nondestructive electrochemical methods.

Acknowledgements

The authors acknowledge LANNBIO for permitting the use of their facilities, as well as to M. Sci. Dora Huerta and W. J. Cauich-Ruiz for their technical assistance in data acquisition.

Funding sources

This research was funded by Centro Mexicano de Inovación en Energía del Océano (CEMIE) grant number [00249795]. Luis Chávez gratefully thanks CONACYT for his scholarship as M.Sci. student at CINVESTAV-IPN.

Author details

Gloria Acosta, Lucien Veleva*, Luis Chávez and Juan L. López
Applied Physics Department, Research Center for Advanced Study (CINVESTAV-IPN), Mérida, Yucatán, México

*Address all correspondence to: veleva@cinvestav.mx

References

[1] Davis JR. Understanding the Basics. Ohio: ASM International; 2001. 351 p. DOI: 10.1361/autb2001p351

[2] Altenpohl DG. Aluminum Viewed from Within: An Introduction into the Metallurgy of Aluminum Fabrication. Düsseldorf: Aluminum-Verlag; 1982

[3] Pourbaix M. Atlas of Electrochemical Equilibria in Aqueous Solutions. Huston, TX: NACE International; 1974

[4] Szklarska-Smialowska Z. Pitting corrosion of aluminum. Corrosion Science. 1999;**41**:1743-1767. DOI: 10.1016/S0010-938X(99)00012-8

[5] Tiryakioğlu M, Staley J. Physical metallurgy and the effect of alloying additions in aluminum alloys. In: Totten GE, MacKenzie DS, editors. Handbook of Aluminum. New York: Marcel Dekker, Inc; 2003. pp. 81-210

[6] Reboul MC, Baroux B. Metallurgical aspects of corrosion resistance of aluminium alloys. Materials and Corrosion. 2011;**62**:215-233. DOI: 10.1002/maco.201005650

[7] Mutombo K. Intermetallic particles-induced pitting corrosion in 6061-T651 aluminium alloy. Materials Science Forum. 2011;**690**:389-392. DOI: 10.4028/www.scientific.net/MSF.690.389

[8] Guillaumin V, Mankowski G. Localized corrosion of 2024 T351 aluminium alloy in chloride media. Corrosion Science. 1999;**41**:421-438. DOI: 10.1016/S0010-938X(98)00116-4

[9] Gharavi F, Matori K, Yunus R, Othman NK, Fadaeifard F. Corrosion evaluation of friction stir welded lap joints of AA6061-T6 aluminum alloy. Transactions of Nonferrous Metals Society of China. 2016;**26**:684-696. DOI: 10.1016/S1003-6326(16)64159-6

[10] Zheng Y, Luo B, Bai Z, Wang J, Yin Y. Study of the precipitation hardening behavior and intergranular corrosion of Al-Mg-Si alloy with differing Si contents. Meta. 2017;**7**:387-399. DOI: 10.3390/met7100387

[11] F-l Z, Z-l W, Li J-f, Li C-x, Tan X, Zhang Z, et al. Corrosion mechanism associated with Mg_2Si and Si particles in Al—Mg—Si alloys. Transactions of Nonferrous Metals Society of China. 2011;**21**:2559-2567. DOI: 10.1016/S1003-6326(11)61092-3

[12] Birbilis N, Buchheit RG. Electrochemical characteristics of intermetallic phases in aluminum alloys an experimental survey and discussion. Journal of the Electrochemical Society. 2005;**152**:B140-B151. DOI: 10.1149/1.1869984

[13] McCafferty E. Sequence of steps in the pitting of aluminum by chloride ions. Corrosion Science. 2003;**5**:1421-1438. DOI: 10.1016/S0010-938X(02)00231-7

[14] Burstein GT, Liu C, Souto RM, Vines SP. Origins of pitting corrosion. Corrosion Engineering, Science and Technology. 2004;**39**:25-30. DOI: 10.1179/147842204225016859

[15] Liang M, Melchers R, Chaves I. Corrosion and pitting of 6060 series aluminium after 2 years exposure in seawater splash, tidal and immersion zones. Corrosion Science. 2018;**140**:286-296. DOI: 10.1016/j.corsci.2018.05.036

[16] LaQue FL. Marine Corrosion: Causes and Prevention. New York: John Wiley & Sons; 1975

[17] Al-Fozan SA, Malik AU. Effect of seawater level on corrosion behavior of different alloys. Desalination. 2008;**228**:61-67. DOI: 10.1016/j.desal.2007.08.007

[18] Roberge PR. Handbook of Corrosion Engineering. New York: McGraw-Hill; 2000

[19] Dawson JL. Electrochemical noise measurement: The definitive in-situ technique for corrosion applications. In: Kearns J, Scully J, Roberge P, Reichert D, Dawson JL, editors. Electrochemical Noise Measurement for Corrosion Applications. West Conshohocken, PA: ASTM STP 1277; 1996. pp. 3-35. DOI: 10.1520/STP37949S

[20] Xia DH, Song SZ, Behnamian Y. Detection of corrosion degradation using electrochemical noise (EN): Review of signal processing methods for identifying corrosion forms. Corrosion Engineering, Science and Technology. 2016;**51**:527-544. DOI: 10.1179/1743278215Y.0000000057

[21] Casajús P, Winzer N. Electrochemical noise analysis of the corrosion of high-purity Mg–Al alloys. Corrosion Science. 2015;**94**:316-326. DOI: 10.20964/2018.01.86

[22] Lee CC, Mansfeld F. Analysis of electrochemical noise data for a passive system in the frequency domain. Corrosion Science. 1998;**40**:956-962. DOI: 10.1016/j.arabjc.2012.02.018

[23] Roberge PR. Quantifying the stochastic behavior of electrochemical noise measurement during the corrosion of aluminum. In: Kearns JR, Scully JR, Roberge PR, Reichert DL, Dawson JL, editors. Electrochemical Noise Measurement for Corrosion Applications. West Conshohocken, PA: ASTM STP 1277; 1996. pp. 142-156. DOI: 10.1520/STP37957S

[24] Eke A, Hermán P, Bassingthwaighte JB, Raymond GM, Percival DB, Cannon M, et al. Physiological time series: Distinguishing fractal noises from motions. European Journal of Physiology. 2000;**439**: 403-415. DOI: 10.1007/s004249900135

[25] Delignieres D, Ramdani S, Lemoine L, Torre K, Fortes M, Ninot G. Fractal analyses for 'short' time series: A re-assessment of classical methods. Journal of Mathematical Psychology. 2006;**50**:525-544. DOI: 10.1016/j.jmp.2006.07.004

[26] Planinšič P, Petek A. Characterization of corrosion processes by current noise wavelet-based fractal and correlation analysis. Electrochimica Acta. 2008;**53**:5206-5214. DOI: 10.1016/j.jmp.2006.07.004

[27] López JL, Veleva L, López-Sauri DA. Multifractal detrended analysis of the corrosion potential fluctuations during copper patina formation on its first stages in sea water. International Journal of Electrochemical Science. 2014;**9**: 1637-1649

[28] Acosta G, Veleva L, López JL. Power spectral density analysis of the corrosion potential fluctuation of aluminium in early stages of exposure to Caribbean sea water. International Journal of Electrochemical Science. 2014;**9**: 6464-6474

[29] Acosta G, Veleva L, López JL, López-Sauri DA. Contrasting initial events of localized corrosion on surfaces of 2219-T42 and 6061-T6 aluminum alloys exposed in Caribbean seawater. Transactions of Nonferrous Metals Society of China. 2019;**29**:34-42

[30] Mena-Morcillo E, Veleva LP, Wipf DO. Multi-scale monitoring the first stages of electrochemical behavior of AZ31B magnesium alloy in simulated body fluid. Journal of the Electrochemical Society. 2018; **165**:C749-C755. DOI: 10.1149/2.0291811jes

[31] McCabe WL, Smith JC, Harriott P. Unit Operations of Chemical Engineering. 4th ed. New York: McGraw Hill; 1985

[32] ASTM G1−90. Standard practice for preparing, cleaning, and evaluation corrosion test specimens

[33] ASTM G199-09. Standard guide for electrochemical noise measurement

[34] Stein JY. Digital Signal Processing: A Computer Science Perspective. 2nd ed. New York: John Wiley & Sons; 2000

[35] Yasakau KA, Zheludkevich ML, Ferreira MGS. Role of intermetallics in corrosion of aluminum alloys. In: Mitra R, editor. Smart Corrosion Protection. Aveiro, Portugal: Woodhead Publishing; 2018. 425 p. DOI: 10.1016/B978-0-85709-346-2.00015-7

[36] Ender VV, Wetzel C. Gross-Kraftwerkbret: VGB Tech. Ver; 1998, R 6/1-R6/20

[37] Afzal SN, Shaikh MA, Mustafa CM, Nabi M, Ehsan MQ, Khan AH. Study of aluminum corrosion in chloride and nitrate media and its inhibition by nitrite. Journal of Nepal Chemical Society. 2006;**22**:26-33. DOI: 10.3126/jncs.v22i0.519

[38] Foley RT, Nguyen TH. The chemical nature in aluminum corrosion, V. energy transfer in aluminum dissolution. Journal of the Electrochemical Society. 1982;**129**: 464-467. DOI: 10.1149/1.2123881

[39] Brown RR, Daut GE, Mrazek RV, Gokcen NA. Solubility and Activity of Aluminum Chloride in Aqueous Hydrochloric Acid Solutions. Washington, DC: U.S. Department of the Interior, Bureau of Mines; 1979

[40] Nikseresht Z, Karimzadeh F, Golozar MA, Heidarbeigy M. Effect of heat treatment on microstructure and corrosion behavior of Al6061 alloy weldment. Materials and Design. 2010; **31**:2643-2648. DOI: 10.1016/j.matdes.2009.12.001

[41] Zhu Y, Sun K, Frankel GS. Intermetallic phases in aluminum alloys and their roles in localized corrosion. Journal of the Electrochemical Society. 2018;**165**:C807. DOI: 10.1149/2.0931811jes

[42] Ghali E. General, galvanic, and localized corrosion of aluminum and its alloys. In: Winston Revie R, editor. Corrosion Resistance of Aluminum and Magnesium Alloys: Understanding, Performance, and Testing. Hoboken, New Jersey: John Wiley & Sons; 2010. 176 p. DOI: 10.1002/9780470531778.ch5

[43] John FM, William FS, Peter ES, Kenneth DB. In: Chastain J, editor. Handbook of X-ray Photoelectron Spectroscopy. Minnesota: Physical Electronics; 1992. pp. 44-55

[44] Loto CA. Electrochemical noise measurement technique in corrosion research. International Journal of Electrochemical Science. 2012;**7**: 9248-9270

[45] Malo JM, Velazco O. Elecrochemical noise response of steel under hydrodynamic conditions. In: Kearns JR, Scully JR, Roberge PR, Reichert DL, Dawson JL, editors. Electrochemical Noise Measurement for Corrosion Applications. West Conshohocken, PA: ASTM STP 1277; 1996. pp. 387-397. DOI: 10.1520/STP37972S

[46] Sanchez-Amaya JM, Cottis RA, Botana FJ. Shot noise and statistical parameters for the estimation of corrosion mechanisms. Corrosion Science. 2005;**47**:3280-3299. DOI: 10.1016/j.corsci.2005.05.047

[47] Curioni M, Cottis RA, Thompson GE. Application of electrochemical noise analysis to corroding aluminium alloys. Surface and Interface Analysis. 2013;**45**:1564-1569. DOI: 10.1002/sia.5173

[48] G102-89. Standard practice for calculation of corrosion rates and related information from electrochemical measurements

[49] Eden DA, John DG, Dawson JL. Corrosion monitoring: WIPO Patent, 1987, 19871107022. 1987. pp. 11–19